



## Spatially propagating activation of quorum sensing in *Vibrio fischeri* and the transition to low population density

Keval Patel <sup>1</sup>, Coralis Rodriguez,<sup>2</sup> Eric V. Stabb,<sup>2,3</sup> and Stephen J. Hagen <sup>1,\*</sup>

<sup>1</sup>*Physics Department, University of Florida, Gainesville, Florida 32611-8440, USA*

<sup>2</sup>*Department of Microbiology, University of Georgia, Athens, Georgia 30602, USA*

<sup>3</sup>*Department of Biological Sciences, University of Illinois, Chicago, Illinois 60607, USA*



(Received 2 February 2020; accepted 5 May 2020; published 26 June 2020)

Bacteria communicate by secreting and detecting diffusible small molecule signals or pheromones. Using the local concentrations of these signals to regulate gene expression, individual cells can synchronize changes in phenotype population-wide, a behavior known as quorum sensing (QS). In unstirred media, the interplay between diffusion of signals, bacterial growth, and regulatory feedback can generate complex spatial and temporal patterns of expression of QS-controlled genes. Here we identify the parameters that allow a local signal to trigger a self-sustaining, traveling activation of QS behavior. Using the natural bioluminescence of wild-type *Vibrio fischeri* as a readout of its *lux* QS system, we measure the induction of a spreading QS response by a localized triggering stimulus in unstirred media. Our data show that a QS response propagates outward, sustained by positive feedback in synthesis of the diffusible signal, and that this response occurs only if the triggering stimulus exceeds a critical threshold. We also test how the autonomous or untriggered activation of the *V. fischeri* QS pathway changes at very low initial population densities. At the lowest population densities, clusters of cells do not transition to a self-sensing behavior, but rather remain in communication via signal diffusion until they reach sufficiently large size that their own growth slows. Our data, which are reproduced by simple growth and diffusion simulations, indicate that in part owing to bacterial growth behavior, natural QS systems can be characterized by long distance communication through signal diffusion even in very heterogeneous and spatially dispersed populations.

DOI: [10.1103/PhysRevE.101.062421](https://doi.org/10.1103/PhysRevE.101.062421)

### I. INTRODUCTION

Many species of bacteria communicate using diffusible small molecule signals or pheromones. Individual cells secrete the signals into their environment, leading to a rising local concentration that other cells detect through dedicated receptors that control important regulatory pathways. This form of intercellular communication, known as quorum sensing (QS), allows bacteria to detect and respond collectively to their own population density and to other environmental parameters such as stress conditions, competition from other microbial species, and symbiotic or host-pathogen interactions [1,2].

The gene regulatory pathways associated with QS typically possess complex architecture. Synthesis of the diffusible signal is often regulated with positive feedback, so that production of a signal accelerates when its local concentration attains a certain threshold [1]. QS pathways also typically respond to multiple chemical signals and to cross-species interactions. As a result regulatory pathways controlled by QS may have elaborate sensing capabilities and dynamics whose biological consequences are unclear [3,4]. Researchers in synthetic biology have demonstrated some of this potential by engineering QS bacteria and assemblies that exhibit pattern

formation, oscillations, and other types of reaction-diffusion phenomena [5–7]. Manipulating QS bacteria into specific configurations or confining them in microfluidic structures can also produce interesting behaviors [8–11].

Even wild-type bacteria under unstirred conditions, where the intercellular signals travel only by diffusion, can demonstrate striking spatial and temporal effects in QS. The interaction between colony growth, signal diffusion, and other phenomena can generate traveling wave fronts of quorum activation [12], pulsing and synchrony over large distances [13], and percolationlike thresholds of activation [14]. The behavior of QS systems in the absence of advection has been analyzed through simple modeling that considers generic properties of QS regulatory pathways [12,15–18], as well as effects such as cell positioning [19] and spreading [20]. Such modeling indicates, for example, that activation of a QS pathway can, in principle, propagate in wavelike fashion through a spatially dispersed population [17]. Modeling also suggests that QS activation may differ qualitatively in more homogeneous, uniformly distributed populations than in heterogeneous, clustered populations: several models propose that cells within isolated high density clusters may activate their QS pathways more rapidly than they would in more dispersed or homogeneous configurations [4,16,18,19].

Surprisingly, however, the connection to experimental data is incomplete. In particular there are few data on the conditions that are required to trigger a traveling activation [13,17]

\*sjhagen@ufl.edu

of the QS pathway of a natural bacterial system. The lack of data makes it difficult to answer key biological questions, such as what kind of local environmental stimulus can, by diffusion of QS signals, elicit a response from distantly located cells that encounter a different environment [21]. There is also little experimental evidence to support the model scenario [15,16] in which a tight cluster of cells attains rapid QS activation by self-sensing, rather than by exchanging signal (communicating) with neighbors.

Here we investigate experimentally the conditions required for *Vibrio fischeri* bacteria to exhibit a spatially spreading response to a localized stimulus when the cells are embedded in a semisolid medium. Using a wild-type strain and its natural bioluminescence as a readout of QS activation, we also test how the timescale for endogenous (absent an external stimulus) autoinduction of the QS pathway is affected by dispersion of the population to very low and heterogeneous density.

## II. METHODS

### A. Construction and growth of strains

*V. fischeri* strain MJ11 is a brightly luminescent wild-type strain [22]. Strain NL63 is a mutant of *V. fischeri* strain ES114 that is unable to produce 3OC6-HSL or C8-HSL owing to a frameshift mutation and deletion, respectively, of the corresponding synthase genes *luxI* and *ainS* [23]. Strains CR5 and CR6 are derived from *V. fischeri* strain KV6576 (an ES114 derivative) [24]. They contain *gfp* embedded in the *lux* operon between *luxI* and *luxC* to act as a reporter [25]. CR5 contains a functional copy of the *luxI* gene that enables 3OC6-HSL synthesis, whereas CR6 does not. The CR5 and CR6 strains were generated by allelic exchange, with alleles introduced by triparental mating, as described previously [26,27], and the mutant loci were confirmed by polymerase chain reaction (PCR) and DNA sequencing. To generate the alleles on mobilizable plasmids, the *gfp* variant in pJLS198 was PCR amplified using primers JLSsrA-ASV [25] and CRG3 (5'-ATTAGCGGCC GCGAAGGAGA TATACATATG GCTAGCAAAG GAGAAGAAC -3'), the amplicon was digested with NotI and BamHI, and the resulting fragment was cloned into similarly digested pJLB72 [27] to place *gfp* between flanking *luxI* and *luxC* fragments. The *luxI-gfp-luxC* allele on the resulting plasmid, pCRG4, was exchanged into KV6576 to generate CR5. The *luxI* gene in pCRG4 was inactivated by digesting a unique BglII site within the gene, filling in the 4-base pair overhangs, and religating to generate a frameshift mutation, thereby generating pCRG23. The mutant *lux* allele in pCRG23 was exchanged into the genome of CR5 to generate CR6. MJ11 and ES114 are distinct natural isolates of *V. fischeri* and carry different *luxR* alleles as well as differences in the *lux* regulatory region [28].

*V. fischeri* were cultured overnight in a complex medium based on seawater and tryptone (SWTO) [29] and then diluted 100× into fresh SWTO. After cells had grown to an optical density (OD) of 0.3 (in 1 cm at 600 nm), corresponding to  $\approx 3 \times 10^8$  colony forming units (cfu)  $\text{cm}^{-3}$ , the culture was washed three times in defined minimal medium (DMM) [30] to remove  $\sim 99.99\%$  of any endogenously produced homoser-

ine lactone (HSL). Vortexing 70  $\mu\text{L}$  of this culture into 7  $\text{cm}^3$  growth medium (DMM or conditioned SWTO) containing 1% (by weight) low-melting-point agarose (Thermo Fisher R0801) at 35°C gave an initial culture density of  $n_0 \approx 1.4 \times 10^6$  cfu  $\text{cm}^{-3}$ . Higher dilution was used to obtain lower  $n_0$ . The agarose-medium + culture mixture was then poured into a 60 mm diameter plate which was cooled for 20 min in a humid, room temperature enclosure prior to imaging.

Conditioned SWTO (c-SWTO) was prepared by growing NL63 in SWTO to OD = 0.25 (in 1 cm at 600 nm) and then filter sterilizing the SWTO. Conditioning removes a molecule present in rich growth media that is inhibitory of *lux* expression [31]. We used a commercial well plate reader (BioTek Synergy 2) to measure the MJ11 growth doubling time as 41 min in c-SWTO-agarose and 116 min in DMM-agarose. [Growth rate  $k = \ln(2)/(\text{doubling time})$ ].

For an exogenous stimulus to *lux* activation, we dissolved 3OC6-HSL or C8-HSL (CAS 143537-62-6, CAS 147852-84-4, Cayman Chemical) in low-melt agarose-medium and then deposited 2  $\mu\text{L}$  of this mixture at the center of the agarose plate. The sample was then cooled for 5 min to allow the agarose to solidify, prior to imaging.

### B. Time-lapse imaging

For imaging bioluminescence, cooled agarose-medium plates were inverted and placed inside a humidified light-proof enclosure with a circulating fan at 23°C. Images of MJ11 were collected every 15 min using a 1024 × 768 pixel, monochrome CCD camera (Imaging Source, DMK31BF03) and 8 s (c-SWTO) or 30 s (DMM) exposure with a 6 mm, f/1.4 lens. Images of CR5 and CR6 were collected using 10 min exposures of a 1392 × 1040 pixel, cooled monochrome CCD camera (Andor Clara) with a 35 mm, f/2 lens, with 5 min between successive exposures. Weighing the plates before and after each experiment showed that evaporative loss was 3% ± 1%. Images were analyzed in MATLAB (Mathworks).

### C. Simulation

We numerically simulated a model in which bacteria embedded at random locations in a thin agarose layer grow while exchanging a diffusible quorum signal. The agarose layer was represented by a flat array (400 × 400 × 1) of cubic volume elements of size  $h^3$ , where  $h = 10 \mu\text{m}$ . A small, random subset of locations within the array was chosen for placement of cells, and a Poisson-distributed random number  $N$  of cells was then placed at each of those locations (with  $\langle N \rangle = 3$ ). The Poisson distribution mimics possible aggregation of cells in the source culture. The number of occupied locations was chosen so that the array overall contained an initial population density  $n_0$  (cells  $\text{cm}^{-3}$ ).

Numerical simulation is based on the following model of growth and signal production. The bacteria exhibit logistic growth [32], in which the number of cells  $N$  at a given location (volume element in the simulation) increases according to

$$\frac{dN}{dt} = kN(1 - N/N_{\text{max}}). \quad (1)$$

Here  $k$  is the growth rate ( $1.9 \times 10^{-4} \text{ s}^{-1}$ , or one doubling per hour), and  $N_{\max} = 10^3$  is the carrying capacity, or maximum number of cells allowed per volume element [32].

Each of the  $N$  cells at any location  $(\mathbf{r}, t)$  releases HSL at a rate that depends on the local concentration  $C(\mathbf{r}, t)$  of HSL [33] but declines late in the growth curve, so HSL synthesis increases  $C(\mathbf{r}, t)$  as

$$\frac{\partial C_{\text{synthesis}}}{\partial t} = \frac{\gamma}{h^3} N (1 - N/N_{\max}) \left( r_0 + \frac{C^2}{C^2 + C_1^2} \right). \quad (2)$$

We use  $\gamma = 6 \times 10^{-23} \text{ mole s}^{-1}$  as the maximum rate of HSL synthesis per cell,  $r_0 = 0.01$  to define a basal rate of synthesis, and  $C_1 = 10^{-8} \text{ M}$  as the threshold for activation of the quorum response [34]. The HSL diffuses with a coefficient  $D = 3 \times 10^{-6} \text{ cm}^2 \text{ s}^{-1}$  [35]. Therefore the HSL concentration obeys

$$\frac{\partial C}{\partial t} = D \nabla^2 C + \frac{\partial C_{\text{synthesis}}}{\partial t}. \quad (3)$$

We model self-activation of the population by simultaneously integrating Eqs. (1), (2), and (3) forward in time at each location in the array, using MATLAB. This integration generates separate, time-dependent arrays containing the values of  $N$  and  $C$  at each location. It continues until at least 50% of the cells in the model experience a local HSL concentration that is sufficient to activate the *lux* pathway. That is, the activation time  $t_a$  is defined as the time at which at least half of the population experiences  $C > C_1$ . To simulate induction by exogenous HSL, we apply the initial condition of a Gaussian-shaped  $C(\mathbf{r}, 0)$  centered at  $\mathbf{r} = 0$ , with  $\sigma = 10h$ , and then integrate Eqs. (1), (2), and (3) to find how  $C$  evolves for cells near the origin.

### III. RESULTS AND DISCUSSION

The marine bacterium *V. fischeri* is an important model organism for the study of bacterial QS. It employs a complex QS pathway in its colonization of its symbiotic host animals, which include certain fish and squid species [36,37]. The full QS pathway in *V. fischeri* detects multiple signals and controls diverse phenotypic outputs related to metabolism, motility, colony morphology, and host colonization [38]. However its best-known output is the blue-green bioluminescence of the bacterium, generated and regulated by the *lux* locus, which encodes a classic Gram negative QS system. The *lux* locus includes *luxR* and the divergently transcribed *lux* operon, which comprises *luxI* as well as genes encoding the bacterial luciferase and other enzymes required for bioluminescence [37]. LuxI is the synthase of the quorum signal *N*-3-oxo-hexanoyl homoserine lactone (3OC6-HSL), which diffuses across cellular membranes and is detected by other *V. fischeri* cells via the intracellular receptor LuxR, encoded by *luxR*. LuxR and 3OC6-HSL bind to form a transcriptional activating complex for the *lux* operon; the complex induces the bioluminescence genes in addition to production of additional LuxI. Therefore high concentrations of 3OC6-HSL induce both the bacterial bioluminescence and, via transcriptional positive feedback, increased production of 3OC6-HSL. LuxR can also bind the *N*-octanoyl-L-homoserine lactone (C8-HSL), which *V. fischeri* synthesizes and detects through a separate QS pathway; con-

sequently the *lux*-controlled bioluminescence is subject to cross talk from the C8-HSL signaling pathway.

We first tested how the initial dispersal or colony density of a population of *V. fischeri*, immobilized in a semisolid growth medium, affects the self-activation time of the QS pathway that regulates the native bioluminescence. Wild-type strain MJ11 was grown to exponential phase in liquid media and then embedded in low-melting-point agarose + medium, forming a thin (2.5 mm deep) layer in a 60 mm diameter plate. The time-lapse images in Fig. 1(a) show that, after an interval that depends on the initial culture density  $n_0$  (cfu  $\text{cm}^{-3}$ ), a burst of bioluminescence appears in each plate. The bioluminescence later fades as the cells enter stationary phase. Defining the activation time  $t_a$  as the time at which luminescence exceeds  $1.5 \text{ counts mm}^{-2}$ , we find that  $t_a$  [Figure 1(b)] increases steadily as  $n_0$  decreases from high ( $n_0 \simeq 2 \times 10^6 \text{ cfu cm}^{-3}$ ) to low ( $\simeq 70 \text{ cfu cm}^{-3}$ ) values. At the lower end of this range the initial cell-to-cell distance is calculated to average 2–3 mm. At  $n_0 < 10^4 \text{ cfu cm}^{-3}$  the isolated individual cells have grown into sizable clusters when quorum is reached, giving the bioluminescence images a granular appearance. Thus at this stage the luminescence images show large pixel-to-pixel variances in brightness [Fig. 1(c)]. Nevertheless, across each plate the onset of luminescence remains mostly well synchronized until  $n_0 < 100 \text{ cfu cm}^{-3}$  [Fig. 1(b)].

The trend of  $t_a$  with decreasing  $n_0$  is initially logarithmic [39], as highlighted by the dashed line in Fig. 2. This behavior is consistent with the simplest picture of quorum activation in a well-mixed, exponential-phase culture: The population density  $n$  (cells  $\text{cm}^{-3}$ ) grows as  $n(t) = n_0 \exp(kt)$ , while each cell synthesizes the activating signal at basal rate  $\gamma' = r_0\gamma \text{ moles s}^{-1}$  (Sec. II). If diffusion between cells is rapid enough in relation to HSL synthesis, then the QS circuit activates population-wide when the signal concentration  $C$  reaches the activation threshold  $C_1$ . Thus bioluminescence is triggered at

$$t_a \simeq -\frac{1}{k} \ln \frac{\gamma' n_0}{k C_1} \quad (4)$$

independent of the HSL diffusion coefficient  $D$ . Equation (4) predicts that the slope of the dashed line in Fig. 2 is the inverse of the growth rate  $k$ , and the intercept corresponds to the population density at which quorum activation occurs in a well-stirred culture. The actual value of the slope corresponds to  $k = 2.8 \times 10^{-4} \text{ s}^{-1}$ , which exactly matches the growth rate  $k$  measured in a plate reader (Sec. II), and the  $x$  intercept (at  $n_0 = 7.5 \times 10^8 \text{ cfu cm}^{-3}$ ) is a typical activating density for *V. fischeri* luminescence [40]. Therefore Fig. 1 indicates that diffusion is efficient and the system behaves as well mixed at moderate to large  $n_0$ , with its QS activation controlled by the spatial-average HSL concentration.

Equation (4) should fail, however, when  $n_0$  is low enough that  $t_a$  exceeds the intercellular diffusion time, roughly  $t_D = (Dn_0^{2/3})^{-1}$ . The inset in Fig. 2 compares  $t_a$  and  $t_D$  for our experimental system (using  $D = 3 \times 10^{-6} \text{ cm}^2 \text{ s}^{-1}$ ) and shows that communication by diffusion between dispersed cells or clusters should be too slow to synchronize QS activation if  $n_0 < 10 \text{ cfu cm}^{-3}$ .

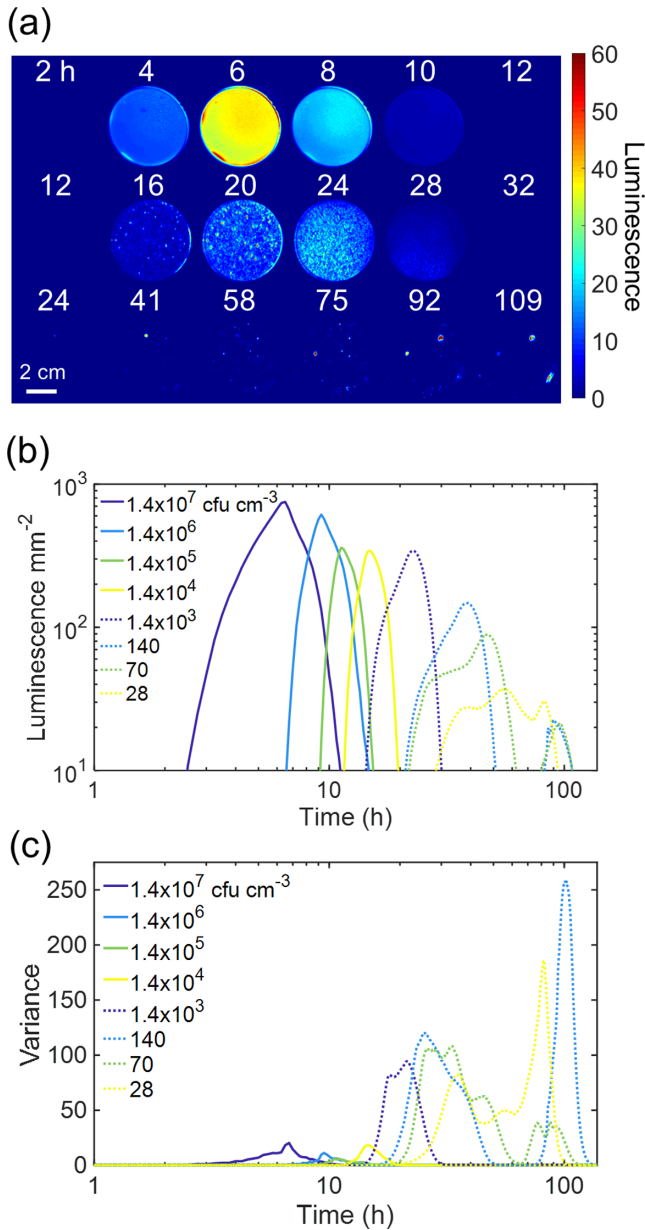


FIG. 1. Autonomous activation of quorum-regulated bioluminescence in MJ11 *V. fischeri* embedded in semisolid medium (c-SWTO + 1% agarose). (a) Bioluminescence imaged at initial population densities  $n_0$  of  $1.4 \times 10^7$  (top row),  $1.4 \times 10^3$  (middle), and 14 (bottom row)  $\text{cfu cm}^{-3}$  at different times as indicated. (b) Luminescence emission from the plates develops at successively later times as the initial  $n_0$  (values indicated) is decreased. (c) Pixel-to-pixel variance in the luminescence images rises sharply for plates prepared with  $n_0 < 10^4 \text{ cfu cm}^{-3}$ , indicating increasing spatial heterogeneity where large cell clusters produce most of the luminescence.

Accordingly, Figs. 1 and 2 show a change in behavior at  $n_0 \simeq 10\text{--}50 \text{ cfu cm}^{-3}$ , where the activation within each plate, as well as the  $t_a$  of plates in different trials, become increasingly variable. At the lowest culture densities ( $n_0 < 10 \text{ cfu cm}^{-3}$ ), where each plate initially contains  $< 10$  cells, the activation time  $t_a$  rises sharply, exceeding 25–40 h.

For unstirred cultures (absent advection and cell motility) different scenarios have been modeled for QS activation at

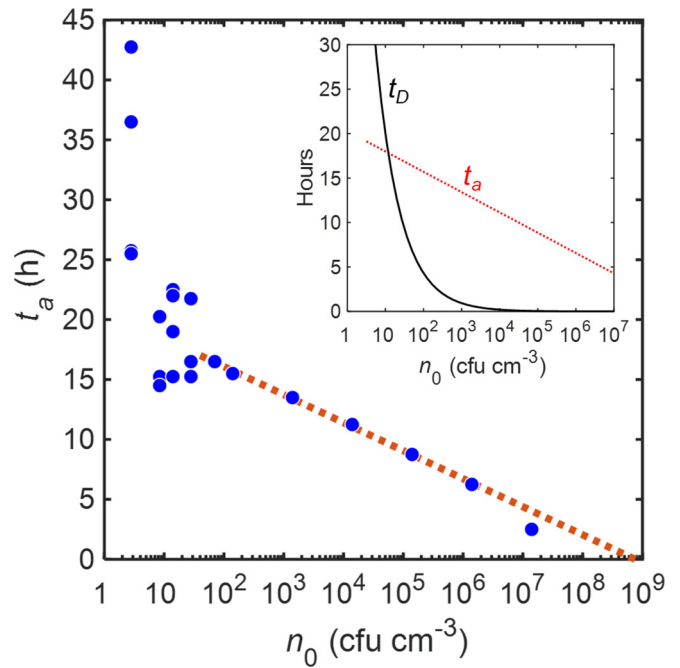


FIG. 2. Time  $t_a$  to bioluminescence activation versus initial culture density  $n_0$ . The dashed line represents  $n_0 \propto \exp -kt_a$  [Eq. (4)] with  $k = 2.8 \times 10^{-4} \text{ s}^{-1}$  and  $kC_1/\gamma' = 7.5 \times 10^8 \text{ cfu cm}^{-3}$ . Inset: Diffusion timescale  $t_D \simeq 1/Dn_0^{2/3}$  (black) exceeds  $t_a$  [Eq. (4), red] for  $n_0 < 10$ .

very low culture densities, where intercell communication becomes inefficient and spatial heterogeneity of the population plays a larger role [4]. Localized groups of cells could, in principle, activate through internal communication even though different groups are uncoupled from each other [18,19]. Alternatively, in a quorum “self-sensing” scenario a solitary cell grows into a compact cluster that eventually triggers its own QS pathway as it secretes its diffusible signal at an exponentially accelerating rate that ultimately overcomes the outward diffusive flux [4,15]. In this scenario, at low  $n_0$  the QS activation behavior transitions from communicating or well mixed ( $t_a \propto -\log n_0$ ) to self-sensing, in which  $t_a$  is sensitive to  $D$  but independent of  $n_0$ .

The observed noise in  $t_a$  at  $n_0 < 50$  is consistent with weakening diffusive coupling between the isolated clusters, so that random variations in cluster size, shape, and proximity lead to chance variability in activation time. However, the eventual divergence of  $t_a$  at the lowest  $n_0$  most likely indicates that QS in a solitary cluster is impeded by the limited rate of nutrient (and  $\text{O}_2$ ) influx as the cluster becomes very large [16], with HSL production declining along with growth. As a result the self-sensing limit is not truly observed; cells remain mostly in communication until activation fails entirely. This transition is examined by simulation below.

We then examined the conditions that allow a pattern of QS activation to spread temporally and spatially through our *V. fischeri*–agarose system. We previously reported that a localized, exogenous HSL stimulus can trigger a spreading *luxIR* response in bacterial cultures that harbor this QS system [13]. Figure 3 shows the stimulation of bioluminescence by a  $2 \mu\text{L}$  droplet of 3OC6-HSL, the primary quorum

signal for *V. fischeri* bioluminescence, which was placed at the plate center ( $r = 0$ ) at  $t = 0$ . Figure 3(a) shows that the CR5 strain (with intact *luxIR* circuit) responds with bioluminescence that propagates steadily outward to  $r \sim 1$  cm [13], at an initial speed of about  $0.1$  cm  $h^{-1}$ . Eventually, the remainder of the plate activates simultaneously. Figure 3(b) shows that the spreading bioluminescence seen in CR5 is not observed in the CR6 strain, which lacks a functional *luxI* encoding the 3OC6-HSL synthase.

The qualitatively different response of the CR5 and CR6 strains is also seen in the shape of the  $(r, t)$  distribution of bioluminescence intensity; the HSL droplet triggers a strong response in CR5 [Fig. 3(c), bottom left], moving outward from  $t = 10$  to  $20$  h, while the CR6 strain shows only a weak transient response to the droplet at  $t \simeq 10$  h [Figure 3(c), bottom right].

The finding that an intact *luxIR* circuit is required for the spreading bioluminescence demonstrates that it is not a passive response of the *lux* operon to the outwardly diffusing HSL droplet, but rather involves the positive-feedback regulated sensing and synthesis of 3OC6-HSL.

In both CR5 and CR6 strains a weak endogenous activation (independent of  $r$ ) of the entire plate is observed at  $t \simeq 19$  h. Its timing is not affected by the triggering HSL droplet or the presence of a functional *luxI*. This activation is presumably due to an accumulation of C8-HSL (synthesized through the *ainSR* pathway) because the CR6 strain cannot produce 3OC6-HSL.

In order to determine the system parameters that control this propagating QS response, we tested the effects of initial colony density and the size of the 3OC6-HSL stimulus in the MJ11 strain. Figure 4(a) shows no spreading response if the amount of added 3OC6-HSL is below a threshold value of a few picomoles. Further, once the provided amount sufficiently exceeds the threshold, the intensity of the bioluminescence (emitted light per unit area) at  $r = 0$  is not greatly increased by additional stimulus [Fig. 4(b)]. By contrast, no amount of the alternative signal C8-HSL elicited a spreading response in the MJ11 strain, and Fig. 4(c) shows no C8-HSL threshold behavior.

Because 3OC6-HSL, but not C8-HSL, participates in the *luxIR* positive transcriptional feedback loop [37], these data are consistent with the exogenous 3OC6-HSL triggering a transient, self-sustaining excitation of 3OC6-HSL synthesis and diffusion, like that modeled in [17]: the *luxIR* circuit is induced in cells where 3OC6-HSL is added, causing them to accelerate their own synthesis of 3OC6-HSL, which diffuses outward to induce *luxIR* in nearby cells.

Figure 4(d) shows that the circuit responds quite abruptly to exogenous 3OC6-HSL exceeding the threshold, although the value of that threshold is only weakly dependent on  $n_0$ . The threshold is also apparent in the activation time  $t_a$ , which varies weakly with the size of the stimulus until the stimulus falls below the threshold value. Below threshold  $t_a$  rises to the self-activation (endogenous HSL) value, more than  $20$  h [Fig. 5(a)].

As Fig. 5(a) shows, the threshold behavior is observed in both DMM and the complex medium SWTO, where growth is more rapid. The threshold is pronounced in the defined medium, where addition of exogenous 3OC6-HSL greater

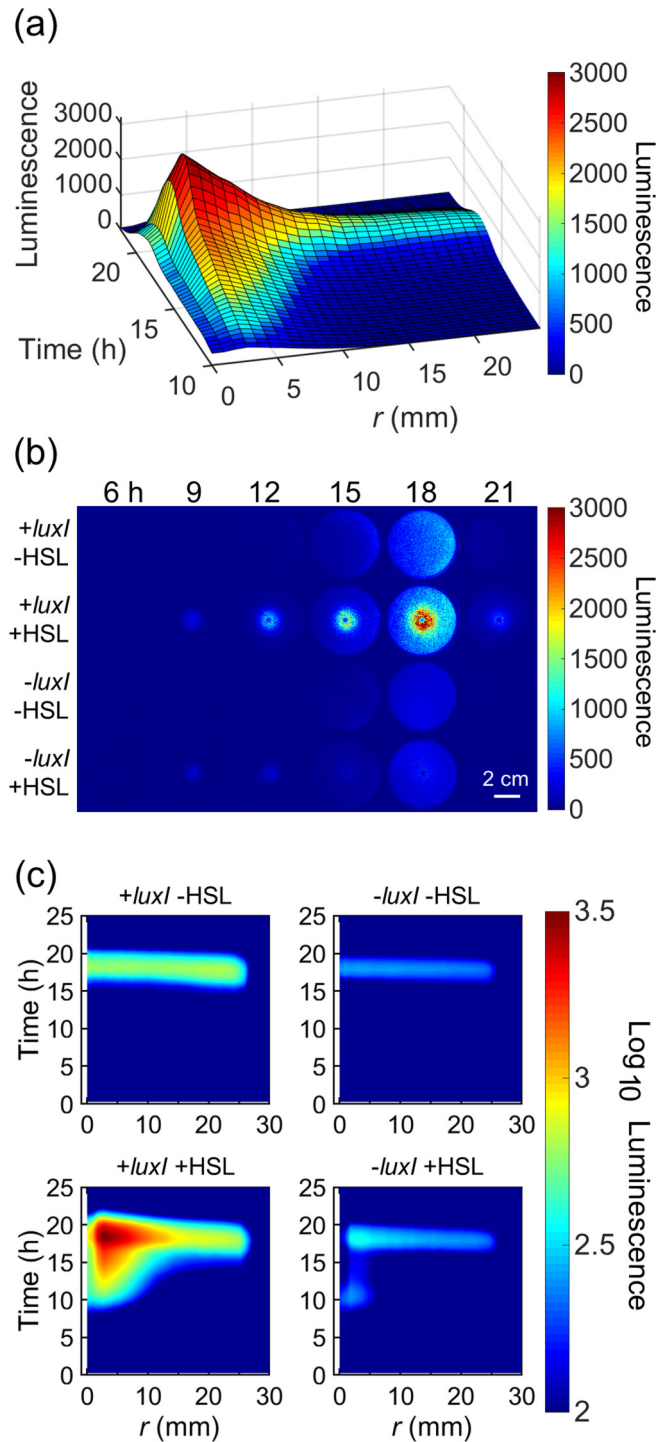


FIG. 3. Spreading bioluminescence of *V. fischeri*, induced by the addition of  $50$  pmol exogenous 3OC6-HSL at  $n_0 = 1.4 \times 10^6$  cfu  $cm^{-3}$ . (a) Bioluminescence of strain CR5 after a 3OC6-HSL droplet is deposited at the plate center  $r = 0$  at  $t = 0$ . (b) Time-lapse images of plates containing strains that possess (CR5, first and second rows) or lack (CR6, third and fourth rows) a functional copy of the gene (*luxI*) encoding the 3OC6-HSL synthase. In the second and fourth rows, a droplet of 3OC6-HSL was added at the plate center at  $t = 0$ . In the first and third rows, no 3OC6-HSL was added. (c) Bioluminescence intensity of CR5 (left) and CR6 (right) versus radial distance  $r$  and time  $t$  from the 3OC6-HSL droplet (bottom row: droplet added; top row: no droplet).

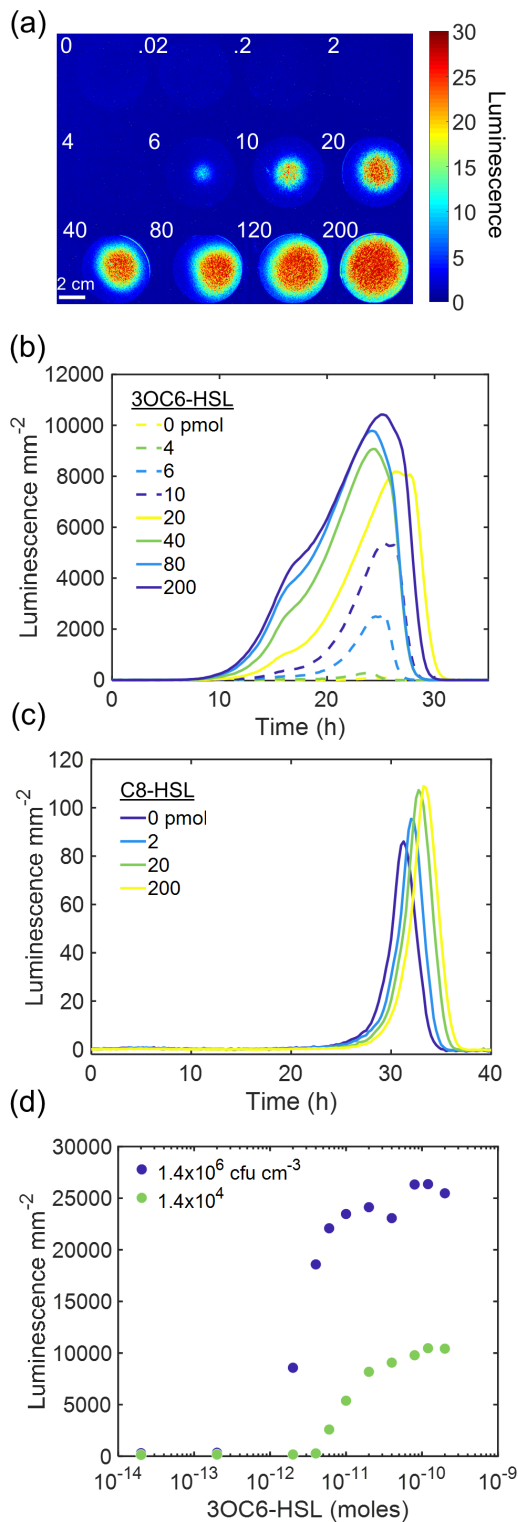


FIG. 4. Threshold behavior of the MJ11 response to exogenously added 3OC6-HSL. Strain MJ11 at  $n_0 = 1.4 \times 10^4$  cfu  $\text{cm}^{-3}$  in DMM is supplied a droplet of 3OC6-HSL at the plate center. (a) Image of plates at  $t = 26$  h for different amounts (given in pmol) of 3OC6-HSL stimulus. (b) The luminescence intensity (luminescence counts/ $\text{mm}^2$ ) at the plate center in response to different 3OC6-HSL stimulus amounts. (c) The luminescence intensity (luminescence counts/ $\text{mm}^2$ ) at the plate center in response to different C8-HSL stimulus amounts. (d) Peak luminescence brightness versus the size of 3OC6-HSL stimulus at high and low  $n_0$ .

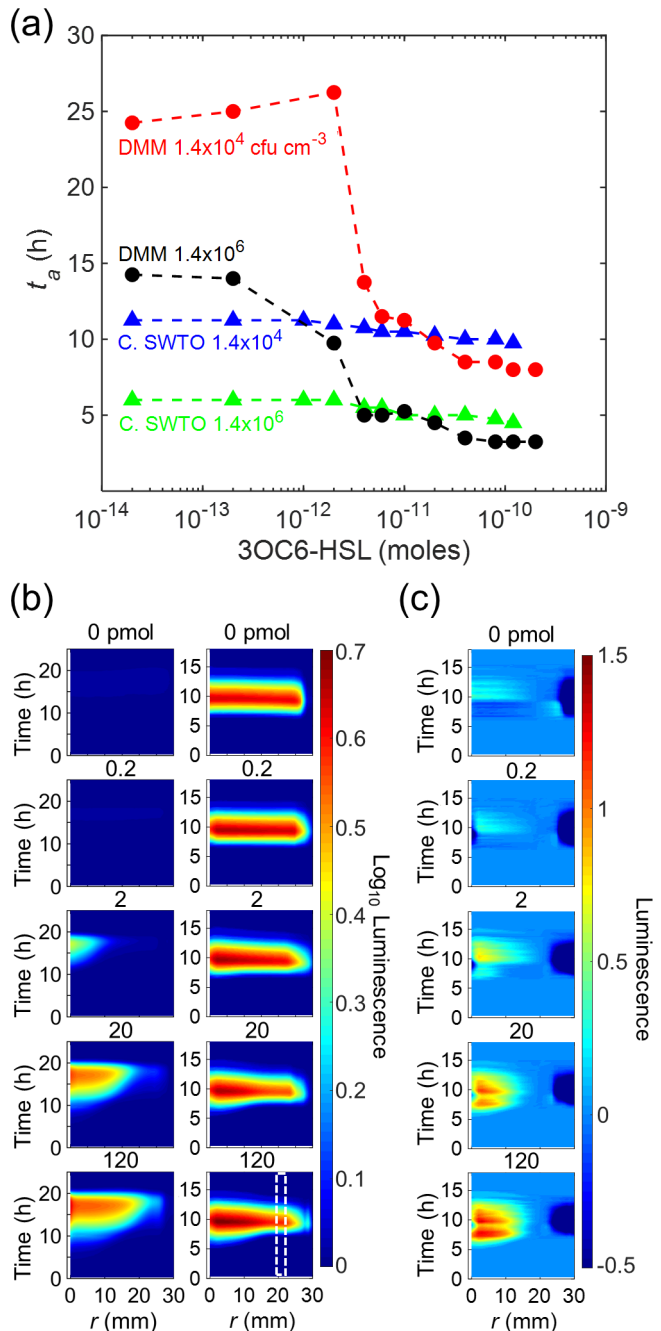


FIG. 5. Effect of initial population density  $n_0$ , growth medium, and added 3OC6-HSL on the time of response for strain MJ11. Data for growth in defined medium (DMM–agarose) and complex medium (c-SWTO–agarose) are shown. (a) Dependence of activation time  $t_a$  on the amount of 3OC6-HSL added at  $\mathbf{r} = 0$ ,  $t = 0$  for MJ11 growing in DMM–agarose and c-SWTO–agarose at high and low  $n_0$ . (b) Threshold response of bioluminescence in DMM–agarose (left column) and c-SWTO–agarose (right column) at  $n_0 = 1.4 \times 10^6$  cfu  $\text{cm}^{-3}$ . The amount of 3OC6-HSL added at  $\mathbf{r} = 0$ ,  $t = 0$  was (from top to bottom) 0, 0.2, 2, 20, 120 pmol. (c) Intensity difference  $I(r, t) - I(2 \text{ cm}, t)$  for MJ11 in c-SWTO, where the bioluminescence far from the droplet is subtracted from each data set in the right column of (b). The white dashed box in the bottom right panel of (b) indicates the region subtracted in (c).

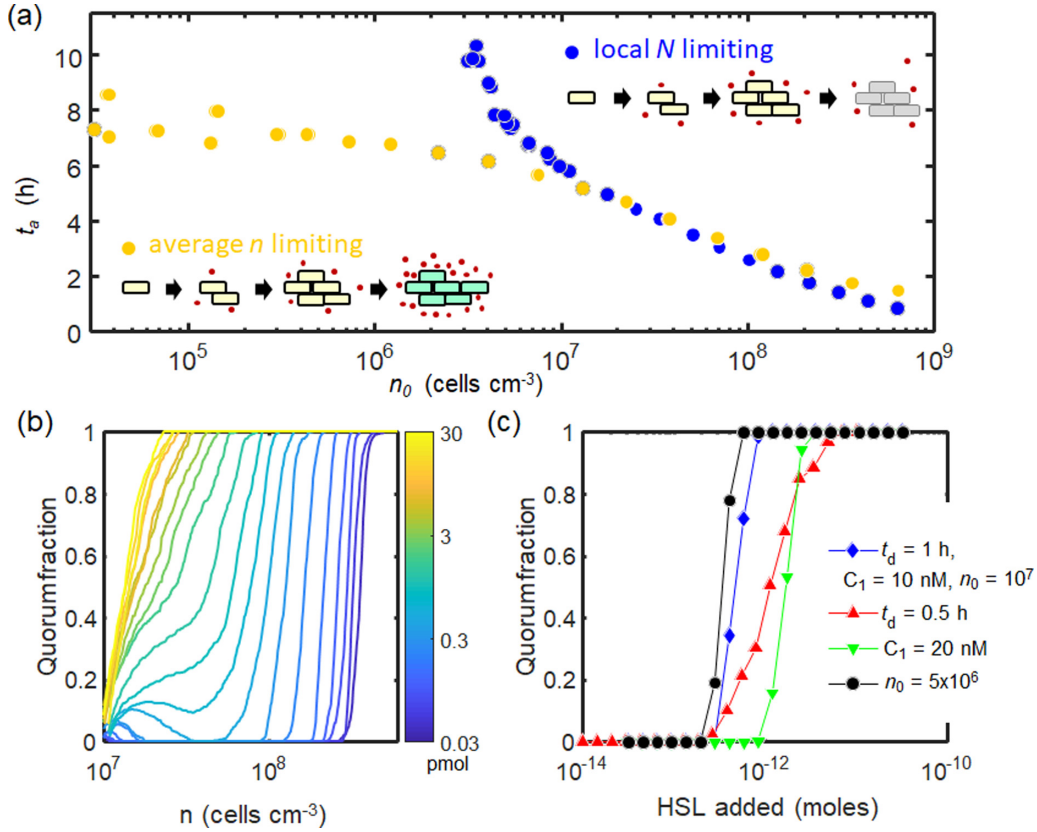


FIG. 6. Simulation of quorum sensing activation of bacteria dispersed in an immobilizing medium. Bacteria secrete diffusible signal [Eq. (2)] during growth [Eq. (1)]. Parameters are given in Sec. II. (a) At high initial population density  $n_0 > 10^7$  cells  $\text{cm}^{-3}$ , the self-activation time  $t_a$  for the culture (in the absence of exogenously added signal) varies as  $t_a \propto -\log n_0$ . Behavior of  $t_a$  at  $n_0 < 10^7$  cells  $\text{cm}^{-3}$  depends on how the late exponential phase of growth is modeled. In an average  $n$  limiting model, where growth is limited by the spatial-averaged population density,  $t_a$  approaches a constant as individual clusters self-activate. However,  $t_a$  diverges in a local  $N$  limiting model, where the rate of growth (and signal synthesis) of an isolated cluster declines as that cluster becomes large. (b) Activation threshold for the quorum circuit by exogenously added signal. Using  $n_0 = 10^7$  cells  $\text{cm}^{-3}$ , different amounts of HSL signal are initially deposited at  $r = 0$ ; the fraction of cells activated is shown versus the spatially averaged population density  $n$  during growth. Activated cells are those for which the local signal concentration exceeds the quorum threshold [ $C(\mathbf{r}, t) > C_1$ ] in Eq. (2). Individual curves are simulations for 20 different quantities of exogenous HSL, logarithmically spaced from  $3 \times 10^{-14}$  to  $3 \times 10^{-11}$  mole, as indicated by the color bar. (c) Effects of doubling time  $t_d = \ln(2)/k$ , signal activation threshold  $C_1$ , and initial population density  $n_0$  on the fraction of the population that is at quorum when  $n = 9 \times 10^7$   $\text{cm}^{-3}$ . The simulation parameters ( $t_d = 1$  h,  $C_1 = 10$  nM,  $n_0 = 10^7$   $\text{cm}^{-3}$ ) used in the first simulation (diamond symbols) are modified in either  $t_d$ ,  $C_1$ , or  $n_0$ , as indicated for the subsequent simulations (upright and inverted triangles, and circles, respectively).

than about 1–3 pmol sharply decreases the activation time [Fig. 5(a)] and qualitatively alters the profile of luminescence vs  $(r, t)$  [Fig. 5(b)]. The complex medium SWTO must be conditioned (Sec. II) in order for *V. fischeri* to respond to exogenously added 3OC6-HSL [31,41]. In conditioned (c-SWTO) medium, the spreading response to exogenous HSL is just slightly faster than the self-activation of the plate: In Fig. 5(b) the spatial temporal patterns of response in the c-SWTO medium show no radial dependence in the absence of added 3OC6-HSL, but some radial dependence is seen when added 3OC6-HSL exceeds 1–2 pmol, indicating that an outwardly spreading activation from  $r = 0$  has been triggered. The change in the spatial dependence of the bioluminescence at the 3OC6-HSL threshold in c-SWTO is more readily seen by subtracting the  $r = 2$  cm intensity from the intensity at  $(r, t)$ , as in Fig. 5(c).

To test our understanding of the observed transition in self-activation time  $t_a$  as  $n_0$  changes and the origin of the threshold response, we numerically solved a simple model (Sec. II) for quorum activation of randomly dispersed bacterial colonies that communicate by diffusion [Eqs. (1), (2), and (3)]. In the model the number of cells  $N$  at a site undergoes logistic growth, Eq. (1), and each cell secretes HSL (of only one type) at a maximum rate  $\gamma$ . However, the synthesis rate is coupled both to the rate of growth and to the local HSL concentration [16], so that HSL production is subject to positive feedback: HSL production is at basal levels when  $C \ll C_1$ , approaches its maximum rate  $\gamma$  if  $C \gg C_1$  and  $N \ll N_{\max}$ , and declines as  $N \rightarrow N_{\max}$  [Eq. (2)]. Here  $C \simeq C_1$  defines the activation threshold for the QS circuit.

Figure 6(a) shows the endogenous (no external HSL stimulus) QS activation time (at which  $C = C_1$ ) obtained in

simulations of the model. Two different cases for logistic growth are considered. In the “local  $N$  limiting” case, growth and HSL synthesis by a cell cluster diminish as the size  $N$  of the cluster approaches the carrying capacity  $N_{\max}$ , as in Eqs. (2) and (1). For low  $n_0$ , this scenario causes HSL synthesis by an isolated cell cluster to decline before the cluster is able to activate its QS circuit. Consequently,  $t_a$  diverges at small  $n_0$ ; no self-activation is observed for  $n_0$  less than about  $3 \times 10^6$  cells  $\text{cm}^{-3}$ .

Figure 6(a) also shows self-activation in an “average  $n$  limiting” case, where it is the spatially averaged density  $\langle n \rangle$  that limits growth and HSL synthesis. Equation (1) is modified to

$$\frac{dN}{dt} = kN \left( 1 - \frac{\langle n \rangle}{n_{\max}} \right), \quad (5)$$

and Eq. (2) for  $\partial C_{\text{synthesis}}/\partial t$  is modified similarly. For low  $n_0$  this model allows an isolated cell cluster to grow far larger before its growth and HSL synthesis slow down.

In this average limiting case an isolated cluster comprising  $N = \exp(kt)$  cells, each of physical size  $\sim a$ , can sustain a quorum-activated state when its own synthesis of HSL is sufficient to maintain a local HSL concentration exceeding  $C_1$  despite the outward diffusing flux. This should be possible when  $N$  reaches

$$4\pi C_1 D N^{1/3} a \simeq \gamma N, \quad (6)$$

which occurs at time

$$t_a \simeq \frac{3}{2k} \ln \frac{4\pi C_1 D a}{\gamma}, \quad (7)$$

which is independent of  $n_0$ . This is the self-sensing [4,15,16] limit. Given our simulation parameters, Eq. (7) predicts a self-sensing  $t_a \simeq 6$  h, which is in agreement with the red points in Fig. 6(a).

Using Eq. (7), we can estimate the self-sensing  $t_a$  for real MJ11. Equation (4) and the slope and intercept of Fig. 2 indicate that  $\gamma/C_1 \simeq 3.7 \times 10^{-13}$   $\text{cm}^3 \text{s}^{-1} \text{cell}^{-1}$  for MJ11, which predicts  $t_a \simeq 7/k = 7$  h. This value is not in agreement with the experimental Fig. 2, where  $t_a$  diverges as  $n_0$  declines, rather than approaching a constant. Therefore the behavior of MJ11 is inconsistent with self-sensing. Arguably, the true activation condition may be more stringent than Eq. (7) because the local  $C$  must already exceed  $C_1$  in order for the maximum HSL synthesis rate to be achieved. However, this hysteresis effect should only delay, not prevent outright, the onset of self-sensing.

The divergence of the measured  $t_a$  at low  $n_0$  is better captured by the local  $N$  limiting model [blue points in Fig. 6(a)], suggesting that the self-limiting nature of bacterial growth tends to prevent crossover from communicating to self-sensing behavior as clusters become more isolated. Presumably, in the real system at low  $n_0$ , random variability in cluster shape, proximity to neighbors and to the plate boundaries and surface, and stochasticity in the HSL response [41] all increase the experimental variability in  $t_a$  beyond what is considered in the simulation.

The model also reproduces the experimentally observed threshold response to an exogenous HSL stimulus. Figure 6(b) shows a simulation of cells growing in a  $0.4 \times 0.4 \text{ cm}^2$  region

(of thickness  $h = 10 \text{ }\mu\text{m}$ ) whose center is initially seeded with a small droplet of diffusible HSL. The quorum fraction, or proportion of cells that experience  $C(r) \geq C_1$ , rises as the population grows. If the amount of added HSL is small, the quorum fraction initially rises until the droplet has diffused outward and then falls until endogenous activation occurs. For a larger stimulus, HSL production becomes immediately self-sustaining, and the quorum fraction rises monotonically with time. As a result the shape of the curves, especially near  $n \sim 3 \times 10^7 \text{ cm}^{-3}$ , changes qualitatively as the HSL stimulus is increased. When the quorum fraction is plotted as a function of the stimulus size [Fig. 6(c)], a threshold effect is observed much like that in Fig. 4(d).

A dimensional argument suggests that the amount  $m$  (moles) of exogenous HSL required to trigger self-sustaining HSL production in the model should depend on  $\gamma$  (the HSL production rate per cell in moles  $\text{s}^{-1}$ ), the diffusion coefficient  $D$ , and  $C_1$  (the HSL concentration threshold in moles  $\text{cm}^{-3}$ ) as

$$m \propto \frac{C_1^2 D}{\gamma}, \quad (8)$$

where the proportionality constant (dimensions of  $L^4$ ) involves  $n_0$  and geometrical factors like the agarose depth and the size of the HSL droplet. The simulation results in Fig. 6(c) are consistent with the  $C_1^2$  dependence in Eq. (8) and also suggest, consistent with experimental data, that the threshold is independent of the bacterial growth rate  $k$  and fairly insensitive to  $n_0$ . In the experimental data in Fig. 5(a) even a 100-fold change in  $n_0$  had little effect on the threshold (a few picomoles) in DMM or c-SWTO.

Overall, our data, together with simple simulations, demonstrate that a propagating QS response in wild-type *V. fischeri* occurs when an exogenous 3OC6-HSL stimulus exceeds a threshold value and is sustained by positive feedback within the *lux* system. The data also indicate somewhat surprisingly that in an unstirred bacterial community intercellular communication through diffusion of the signal is sufficient to synchronize quorum activation of isolated cell clusters, even in very dispersed systems where the signal must diffuse considerable distances between clusters.

#### IV. CONCLUSIONS

Despite the considerable interest in local signaling in QS circuits, our data highlight the importance of longer range diffusive effects in colonies of natural QS bacteria. The spreading QS response observed in a *V. fischeri* colony is a diffusive effect facilitated by positive feedback in HSL synthesis, with a strongly nonlinear property that requires the initial stimulus to exceed a sharp threshold. Notably, the ability of the exogenous stimulus to induce a distinctly propagating response is diminished as the quality of the growth medium increases. Future studies will clarify what parameters define the speed and duration of the response and how these affect the ability of a spatially dispersed population to respond to localized stimuli.

Our data also show that *V. fischeri* QS is characterized by intercolony communication down to very low colony densities. Setting aside murky questions of what an organism



“intends” to detect using QS, there is a physical distinction between the two limits of QS activation by intercolony communication versus autonomous self-sensing by tight aggregates of cells. In the former case the rate of diffusion is not necessarily relevant to the activation timescale. In the latter case efficient diffusion directly inhibits activation. Although modeling of aggregates or clusters (e.g.,  $10^2$ ) of cells dispersed across distances of  $100\ \mu\text{m}$  or greater [18,19] clearly shows a role for spatial distribution and heterogeneity, the rate of diffusion is not necessarily critical to these analyses, and so these models have more in common with the communication limit than the diffusion-controlled self-sensing limit. Nevertheless, our data show that the bacterial growth kinetics have a significant impact on quorum activation at low population densities, an effect that is not always considered in modeling. It is interesting that the finite rate of diffusion, which ultimately enables the self-sensing scenario,

also appears to prevent (because growth requires transport of nutrients and waste products) that scenario from occurring. At least in our experiments growth encounters the diffusion limit just as intercellular communication begins to fail, so that the transition away from intercellular communication is not observed. Interestingly, the coincidence of nutrient or waste product stresses with high local HSL concentration should provide some clue to the individual cells that they are in a highly aggregated, as opposed to highly populated, growth environment. Thus the cells could potentially use the QS circuit to distinguish between the two scenarios.

#### ACKNOWLEDGMENTS

The authors gratefully acknowledge funding support from the National Science Foundation, Grant MCB 1715981.

- 
- [1] W.-L. Ng and B. L. Bassler, Bacterial quorum-sensing network architectures, *Annu. Rev. Genet.* **43**, 197 (2009).
- [2] K. Pappenfort and B. L. Bassler, Quorum sensing signal-response systems in Gram-negative bacteria, *Nat. Rev. Microbiol.* **14**, 576 (2016).
- [3] A. K. Dunn and E. V. Stabb, Beyond quorum sensing: The complexities of prokaryotic parliamentary procedures, *Anal. Bioanal. Chem.* **387**, 391 (2007).
- [4] B. A. Hense, C. Kuttler, J. Müller, M. Rothballer, A. Hartmann, and J.-U. Kreft, Does efficiency sensing unify diffusion and quorum sensing?, *Nat. Rev. Microbiol.* **5**, 230 (2007).
- [5] T. Danino, O. Mondragon-Palomino, L. Tsimring, and J. Hasty, A synchronized quorum of genetic clocks, *Nature (London)* **463**, 326 (2010).
- [6] C. Liu, X. Fu, L. Liu, X. Ren, C. K. Chau, S. Li, L. Xiang, H. Zeng, G. Chen, L.-H. Tang, P. Lenz, X. Cui, W. Huang, T. Hwa, and J.-D. Huang, Sequential establishment of stripe patterns in an expanding cell population, *Science* **334**, 238 (2011).
- [7] J. S. Chuang, Engineering multicellular traits in synthetic microbial populations, *Curr. Opin. Chem. Biol.* **16**, 370 (2012).
- [8] J. Q. Boedicker, M. E. Vincent, and R. F. Ismagilov, Microfluidic confinement of single cells of bacteria in small volumes initiates high-density behavior of quorum sensing and growth and reveals its variability, *Angew. Chem., Int. Ed.* **48**, 5908 (2009).
- [9] E. Carnes, D. Lopez, N. Donegan, A. Cheung, H. Gresham, G. Timmins, and C. Brinker, Confinement-induced quorum sensing of individual *Staphylococcus aureus* bacteria, *Nat. Chem. Biol.* **6**, 41 (2010).
- [10] S. J. Hagen, M. Son, and J. T. Weiss, Bacterium in a box: Sensing of quorum and environment by the *luxI/luxR* gene regulatory circuit, *J. Biol. Phys.* **36**, 317 (2010).
- [11] M. Gao, H. Zheng, Y. Ren, R. Lou, F. Wu, W. Yu, X. Liu, and X. Ma, A crucial role for spatial distribution in bacterial quorum sensing, *Sci. Rep.* **6**, 34695 (2016).
- [12] V. Bettenworth, M. McIntosh, A. Becker, and B. Eckhardt, Front-propagation in bacterial inter-colony communication, *Chaos* **28**, 106316 (2018).
- [13] G. E. Dilanji, J. B. Langebrake, P. De Leenheer, and S. J. Hagen, Quorum activation at a distance: Spatiotemporal patterns of gene regulation from diffusion of an autoinducer signal, *J. Am. Chem. Soc.* **134**, 5618 (2012).
- [14] K. P. T. Silva, T. I. Yusufaly, P. Chellamuthu, and J. Q. Boedicker, Disruption of microbial communication yields a two-dimensional percolation transition, *Phys. Rev. E* **99**, 042409 (2019).
- [15] P. Melke, P. Sahlin, A. Levchenko, and H. Jönsson, A cell-based model for quorum sensing in heterogeneous bacterial colonies, *PLoS Comput. Biol.* **6**, e1000819 (2010).
- [16] B. A. Hense, J. Muller, C. Kuttler, and A. Hartmann, Spatial heterogeneity of autoinducer regulation systems, *Sensors* **12**, 4156 (2012).
- [17] J. B. Langebrake, G. E. Dilanji, S. J. Hagen, and P. D. Leenheer, Traveling waves in response to a diffusing quorum sensing signal in spatially-extended bacterial colonies, *J. Theor. Biol.* **363**, 53 (2014).
- [18] T. I. Yusufaly and J. Q. Boedicker, Spatial dispersal of bacterial colonies induces a dynamical transition from local to global quorum sensing, *Phys. Rev. E* **94**, 062410 (2016).
- [19] O. Kindler, O. Pulkkinen, A. G. Cherstvy, and R. Metzler, Burst statistics in an early biofilm quorum sensing model: The role of spatial colony-growth heterogeneity, *Sci. Rep.* **9**, 12077 (2019).
- [20] D. Quan, C.-Y. Tsao, H.-C. Wu, and W. Bentley, Quorum sensing desynchronization leads to bimodality and patterned behaviors, *PLoS Comput. Biol.* **12**, e1004781 (2016).
- [21] E. V. Stabb, Could positive feedback enable bacterial pheromone signaling to coordinate behaviors in response to heterogeneous environmental cues?, *mBio* **9**, e00098-18 (2018).
- [22] M. J. Mandel, E. V. Stabb, and E. G. Ruby, Comparative genomics-based investigation of resequencing targets in *Vibrio fischeri*: Focus on point miscalls and artefactual expansions, *BMC Genomics* **9**, 138 (2008).
- [23] J. H. Kimbrough and E. V. Stabb, Substrate specificity and function of the pheromone receptor AinR in *vibrio fischeri* ES114, *J. Bacteriol.* **195**, 5223 (2013).

- [24] J. M. Ondrey and K. L. Visick, Engineering *Vibrio fischeri* for inducible gene expression, *Open Microbiol. J.* **8**, 122 (2014).
- [25] J. L. Stoudenmire, T. Essock-Burns, E. N. Weathers, S. Solaimanpour, J. Mrázek, and E. V. Stabb, An iterative, synthetic approach to engineer a high-performance *phob*-specific reporter, *Appl. Environ. Microbiol.* **84**, e00603-18 (2018).
- [26] E. Stabb and E. Ruby, Rp4-based plasmids for conjugation between *Escherichia coli* and members of the Vibrionaceae, *Methods Enzymol.* **359**, 413 (2002).
- [27] J. L. Bose, C. S. Rosenberg, and E. V. Stabb, Effects of *luxCD-ABEG* induction in *Vibrio fischeri*: Enhancement of symbiotic colonization and conditional attenuation of growth in culture, *Arch. Microbiol.* **190**, 169 (2008).
- [28] J. L. Bose, M. S. Wollenberg, D. M. Colton, M. J. Mandel, A. N. Septer, A. K. Dunn, and E. V. Stabb, Contribution of rapid evolution of the *luxR-luxI* intergenic region to the diverse bioluminescence outputs of *Vibrio fischeri* strains isolated from different environments, *Appl. Environ. Microbiol.* **77**, 2445 (2011).
- [29] N. L. Lyell, A. K. Dunn, J. L. Bose, and E. V. Stabb, Bright mutants of *Vibrio fischeri* ES114 reveal conditions and regulators that control bioluminescence and expression of the *lux* operon, *J. Bacteriol.* **192**, 5103 (2010).
- [30] T. Miyashiro, D. Oehlert, V. A. Ray, K. L. Visick, and E. G. Ruby, The putative oligosaccharide translocase SypK connects biofilm formation with quorum signaling in *Vibrio fischeri*, *MicrobiologyOpen* **3**, 836 (2014).
- [31] A. Eberhard, Inhibition and activation of bacterial luciferase synthesis, *J. Bacteriol.* **109**, 1101 (1972).
- [32] S. J. Hagen, Exponential growth of bacteria: Constant multiplication through division, *Am. J. Phys.* **78**, 1290 (2010).
- [33] S. James, P. Nilsson, G. James, S. Kjelleberg, and T. Fagerstrom, Luminescence control in the marine bacterium *Vibrio fischeri*: An analysis of the dynamics of *lux* regulation, *J. Mol. Biol.* **96**, 1127 (2000).
- [34] H. B. Kaplan and E. P. Greenberg, Diffusion of autoinducer is involved in regulation of the *Vibrio fischeri* luminescence system, *J. Bacteriol.* **163**, 1210 (1985).
- [35] A. Trovato, F. Seno, M. Zanardo, S. Alberghini, A. Tondello, and A. Squartini, Quorum vs. diffusion sensing: A quantitative analysis of the relevance of absorbing or reflecting boundaries, *FEMS Microbiol. Lett.* **352**, 198 (2014).
- [36] E. Stabb, A. Schaefer, J. Bose, and E. Ruby, Quorum signaling and symbiosis in the marine luminous bacterium *Vibrio fischeri*, in *Chemical Communication Among Bacteria*, edited by S. Winans and B. Bassler (ASM Press, Washington, DC, 2008), pp. 233–250.
- [37] S. C. Verma and T. Miyashiro, Quorum sensing in the squid-vibrio symbiosis, *Int. J. Mol. Sci.* **14**, 16386 (2013).
- [38] C. Lupp and E. Ruby, *Vibrio fischeri* uses two quorum-sensing systems for the regulation of early and late colonization factors, *J. Bacteriol.* **187**, 3620 (2005).
- [39] M. Barak and S. Ulitzur, The induction of bacterial bioluminescence system on solid medium, *Curr. Microbiol.* **5**, 299 (1981).
- [40] K. H. Nealson, T. Platt, and J. W. Hastings, Cellular control of the synthesis and activity of the bacterial luminescent system, *J. Bacteriol.* **104**, 313 (1970).
- [41] P. D. Perez and S. J. Hagen, Heterogeneous response to a quorum-sensing signal in the luminescence of individual *Vibrio fischeri*, *PLoS ONE* **5**, e15473 (2010).